



Sensitivity and performance enhancement of an SPR biosensor using a gold-silver alloy, zinc oxide and graphene

Innocent Kadaleka Phiri^{1,2} · Mohssin Zekriti¹

Received: 17 April 2024 / Accepted: 25 June 2024 / Published online: 19 July 2024

© The Author(s), under exclusive licence to Springer Science+Business Media, LLC, part of Springer Nature 2024

Abstract

Over the past years, Surface Plasmon Resonance (SPR) has been used in various domains including medical diagnostics, chemical and biological sensing, and environmental monitoring. SPR-based biosensors have more advantages than other optical biosensors due to their rapid, label-free, and targeted detection capabilities. There have been challenges to designing SPR biosensors with enhanced performance and improved environmental adaptability, including considerations such as prism-metal bonding, biomolecule adhesion, and oxidation protection. This paper presents sensitivity and performance enhancement in an SPR biosensor based on Kretschmann configuration while using a low refractive index CaF_2 glass prism, a zinc oxide (ZnO) layer, a gold-silver alloy ($\text{Au}_{10}\text{Ag}_{90}$), and a single layer of 2D graphene. Theoretical analysis shows that the use of a CaF_2 prism and the alloy gives a good sensitivity of $280^\circ/\text{RIU}$. The sole addition of a ZnO layer improves this sensitivity to $320^\circ/\text{RIU}$. Further addition of a graphene layer to make the final proposed structure $\text{CaF}_2/\text{ZnO}/\text{Au}_{10}\text{Ag}_{90}/\text{graphene}/\text{SM}$, improves sensitivity to $340^\circ/\text{RIU}$, giving a figure of merit value of $60.28/\text{RIU}$ and a quality factor value of $102.48/\text{RIU}$. Despite supporting the SPR mode and enhancing sensitivity, ZnO improves prism-alloy bonding while graphene promises better biomolecule adhesion and improved oxidation protection. Overall, our proposed structure has better sensing performance compared to other designs in the literature. The high sensitivity makes our proposed biosensor suitable for the detection of tiny cancer bio-markers in body fluids, enabling early medical interventions.

Keywords Surface plasmon resonance (SPR) · SPR biosensors · Sensitivity enhancement · Gold-silver alloy · Transfer matrix method (TMM) · Biosensing applications

✉ Innocent Kadaleka Phiri
innocentkphiri@gmail.com

✉ Mohssin Zekriti
m.zekriti@ueuromed.org

¹ Euromed Research Center, Euro-Mediterranean University of Fes, Route de Meknes, Rond-Point de Bensouda, B. P. 51, 30030 Fès, Morocco

² Physics and Electronics Department, School of Natural and Applied Sciences, University of Malawi, P. O. Box 280, Zomba, Malawi

1 Introduction

Optical biosensors play a crucial role in chemical and biological sensing by using light and its properties in their detection mechanism. In general, biosensors are analytical devices that detect particular elements, called analytes, in a sample using biological recognition components such as enzymes, antibodies, or DNA, and then they translate this information into a quantifiable output signal (Tetyana et al. 2021). In Surface Plasmon Resonance (SPR) biosensors, the sensing action is based on measuring a shift in refractive index in the very near vicinity of the sensor surface due to analytes binding (Naresh and Lee 2021). According to Homola (2003), SPR biosensors provide rapid, real-time, highly sensitive, label-free, and targeted detection of different biomolecules. These benefits make SPR biosensors superior to label-based biosensors in different fields ranging from medical diagnostics, chemical and biological sensing, food quality, and environmental monitoring.

SPR refers to an optical phenomenon wherein a p-polarized light wave incident on a metal surface induces resonance in electrons near the surface. Resonating coupling between the incident photons and free electrons in the metal is called SPR. This resonance leads to the generation of an oscillating charge-density and an associated evanescent electric field (Barnes 2006; Barnes et al. 2003; Homola et al. 1999). According to Kretschmann and Raether (1968), this resultant field, which decays exponentially, travels along an interface of two media with opposing signs in their real dielectric constants, such as metal and dielectric materials. This field also penetrates evanescently into each of the two media (Gray, 2013; Homola et al. 1999).

Not all materials exhibit plasmonic properties. Rather, this phenomenon is possible in metals with a negative real dielectric constant and a large volume of free electrons such as gold (Au) and silver (Ag) (Homola et al. 1999). According to Otto (1968), Au has strong chemical stability and strong oxidation resistance, whereas Ag produces smaller resonance curves and has higher sensitivity compared to Au. These properties make Au and Ag to be the most commonly utilized metals. Despite this, Au exhibits lower sensitivity and produces a larger resonance curve, while Ag easily oxidizes (Otto 1968; Zekriti 2021). Copper (Cu) and aluminium (Al) also exhibit plasmonic properties, but they suffer from higher losses which cause heavy thermal damping (Cortie et al. 2020).

Due to these challenges, different solutions have been proposed in the literature. To support the SPR mode, Mafazi et al. (2022); Nesterenko et al. (2012) used bimetallic configurations such as Ag–Au, Cu–Au, and Al–Au with Au as the cover layer. Other researchers have replaced the cover metal with a 2D material such as graphene (Gan et al. 2019) and graphene (Zekriti 2021) while using Ag as the primary plasmonic material. Despite supporting SPR and improving oxidation protection, bimetallic structures have been shown to produce lower sensitivity and wider resonance curves affecting sensing performance (Mafazi et al. 2022).

Metal oxides are also used in optical biosensors because of their optical properties and well-controlled deposition process (Kumar et al. 2018; Mostufa et al. 2022). Zinc oxide (ZnO), in particular, has gained popularity in SPR biosensors either as a thin film in Kretschmann configuration or as a shell in localized surface plasmon resonance (Basak et al. 2020; Kumar et al. 2018, 2020). Notably, ZnO is the hardest material among the II–IV semiconductor compounds. Furthermore, ZnO is a low-cost, biocompatible, and biodegradable material, making it a safe choice for biosensing and bio-detection. In contrast to Au and Ag, ZnO does not exhibit the SPR effect due to its large band gap of approximately 3.4 eV, making it transparent to visible light. Stated differently, ZnO lacks free electrons that can couple with incident light

in the visible range. According to Kumar et al. (2018), ZnO has a higher isoelectric point, a larger surface-to-volume ratio, and enhances the capacity for light collection.

One of the challenges faced by SPR biosensors in recent years is to ensure maximum adhesion of the plasmonic metal to the prism. Accordingly, the solution is to place an adhesion layer between these materials. Despite this, Kumar et al. (2023) states that some adhesion layers affect a biosensor's performance by widening the resonance curve and damping its magnitude, causing significant losses and lower sensitivity. Several metals such as Chromium (Cr) and Titanium (Ti) have been used for adhesion purposes. In real-life experience, however, several drawbacks of these metals were observed such as metal inter-diffusion and a low portion of light being transmitted to the surface of the plasmonic layer. Moreover, the use of Cr or Ti can be possible by considering very small thicknesses in such a way that light can easily reach the metal surface. The use of small thicknesses affects the quality of the layer surface and leads to the formation of nano-islands. With this effect, the deposition of Au or Ag with a smooth surface over Cr or Ti becomes challenging. Due to its higher transparency, ZnO is a good alternative compared to conventional materials even with larger thickness for ensuring the adhesion of the metals to the prism.

In Mudgal et al. (2020a), an Ag-based sensor is coated with silicon nitride (Si_3N_4) and then graphene. Si_3N_4 was chosen for its anti-reflection property which is shown to improve sensitivity. In a different approach, higher sensitivity in refractive index sensing can be achieved by the use of multi-mode fiber structures as discussed in Teng et al. (2022).

From this background, we observe some shortfalls of the common structures that affect the design of SPR biosensors. As discussed above, the conventional structures have displayed lower sensitivity and larger resonance curves (when using Au, bimetallic structures, or adhesion layers); weaker oxidation protection (when using Ag); and higher losses (when using Cu or Al). Therefore, there is a need to design a biosensor with improved oxidation resistance and better metal-prism bonding, while producing better sensing performance especially higher sensitivity. In this work, we present a theoretical design of an SPR biosensor using a low refractive index Calcium Fluoride (CaF_2) glass prism and a gold-silver alloy ($\text{Au}_{10}\text{Ag}_{90}$). In our design, we also include additional layers in terms of a ZnO layer between the prism and the alloy, and a graphene layer as the alloy cover. In the physical design, we use the common Kretschmann-based prism configuration. In terms of mathematical design, we use the Transfer Matrix Method (TMM) model implemented in MATLAB. We also use the software Lumerical FDTD to generate electric field distribution profiles. We optimize the thickness of each layer in our design to generate better results. Results show that despite improving prism-alloy bonding, ZnO also supports SPR mode and improves sensitivity. Furthermore, despite improving oxidation protection and biomolecule adhesion properties, a thin graphene film also supports the SPR mode and enhances sensitivity. The use of a low refractive index prism and an alloy improves sensitivity. In general, our proposed design has higher sensitivity, with better figure of merit and quality factor.

This paper is organized as follows: Section 2 presents "Theoretical modelling and design analysis," Section 3 presents "Results and discussion," and finally, Section 4 concludes the paper.

2 Theoretical modelling and design analysis

2.1 Method of SPR excitation

Coupling between incident light and surface plasmons can only occur when the wave vector of incident light parallel to the metal–dielectric interface (designated as k_s) matches the propagation vector of surface plasmons (designated as k_{sp}), which according to Barnes (2006); Barnes et al. (2003); Miyazaki et al. (2017) are given as,

$$k_s = \frac{2\pi}{\lambda} n_p \sin \theta \quad (1)$$

$$k_{sp} = \frac{2\pi}{\lambda} \sqrt{\frac{\epsilon_m \epsilon_d}{\epsilon_m + \epsilon_d}} \quad (2)$$

where λ is the incident light wavelength, n_p is the prism's refractive index, θ is the incidence angle. ϵ_m and ϵ_d are the dielectric constants of the metal and dielectric material, respectively.

This means, there is a need for a coupling method to achieve this matching. Homola (2006); Miyazaki et al. (2017) state three common methods: (1) prism coupling and attenuated total reflection (ATR), (2) diffraction grating method, and (3) use of optical waveguides. Under prism coupling, two common configurations are known: Kretschmann and Otto configurations. The common coupling technique is prism coupling by Kretschmann configuration, where a glass prism is positioned on top of an extremely thin metal film and a dielectric medium (Kretschmann and Raether 1968). Otto configuration describes another setup where the prism and the metal film are separated by an air gap or a dielectric medium (Otto 1968). For all prism coupling methods in general, p-polarized light is incident on one side of the glass prism. Inside the prism, part of the incident light is reflected on the other side of the prism while another portion creates the evanescent wave that penetrates the thin metal film and excites surface plasmons on the outer side of the metal film.

The glass prism is crucial for enabling Total Internal Reflection (TIR) which operates on a defined incidence angle of light known as critical angle (θ_c) that is determined by the properties of the prism and dielectric material. All light is transmitted with zero reflection when it strikes a prism–dielectric interface at incidence angles less than the critical angle ($\theta < \theta_c$); however, all light is reflected when light strikes this interface at incidence angles equal to or greater than the critical angle ($\theta \geq \theta_c$), a scenario called TIR (Knoll 1998; Miyazaki et al. 2017). The TIR angle (θ_{TIR}) equals θ_c and is given by, (Knoll 1998)

$$\theta_{TIR} = \theta_c = \sin^{-1} \sqrt{\epsilon_d / \epsilon_p} \quad (3)$$

where ϵ_p is the dielectric constant of the prism. η_p and ϵ_p are related by $\eta_p = \sqrt{\epsilon_p}$.

Next, when the prism is coated with a plasmonic metal (like Au or Ag) an optical phenomenon known as Attenuated Total Reflection (ATR) occurs. At ATR, most of the incident light is absorbed by the metal leading to a dip on an SPR reflectivity graph. ATR occurs at a specific incidence angle of light where resonance occurs, known as the SPR resonance angle (θ_{SPR}) (Homola 2006; Miyazaki et al. 2017).

The value of θ_{SPR} can be determined from a matching relation: $k_s = k_{sp}$. Thus, using definitions of k_s and k_{sp} from Eqs. (1) and (2), respectively, we get θ_{SPR} as, (Barnes 2006; Barnes et al. 2003; Miyazaki et al. 2017)

$$\theta_{SPR} = \sin^{-1} \sqrt{\frac{\epsilon_m \epsilon_d}{\epsilon_p (\epsilon_m + \epsilon_d)}} \quad (4)$$

Within the context of a bio-sensing experiment, target molecules to be detected (analytes), are introduced in solution through a flow channel. These analytes interact with bio-recognition molecules (known as ligands), which are immobilized on the sensor's surface within a sensing medium (SM). The presence of analytes and any subsequent interaction between analytes and ligands near the sensor's surface result in a change in refractive index. This change can be monitored using different detection techniques including: (1) angular modulation, (2) intensity modulation, and (3) wavelength modulation (Homola et al. 1999; Miyazaki et al. 2017). In angular modulation, for example, the shift in refractive index leads to a corresponding shift in the resonance angle and the reflectivity curve (Homola, 2008).

2.2 Proposed design model and choice of materials

The proposed biosensor model is based on the Kretschmann configuration as shown in Fig. 1 and its physical parameters are shown in Table 1. A discussion on the choice of material for each layer follows.

The first layer is a glass prism. The literature presents different prism types having different refractive indices. According to Karki et al. (2022); Kumar et al. (2018); Uniyal et al. (2022), a lower refractive index produces a larger resonance angle shift, producing larger sensitivity. Due to this, we choose a CaF_2 prism due to its lower refractive index ($n_{\text{CaF}_2} = 1.4329$).

For the plasmonic material, we prefer an alloy due to its enhanced properties. Experimental and analytical studies have shown that some metallic alloys like that of gold-silver (Au–Ag) (Cortie et al. 2020; Rioux et al. 2014) and copper–zinc (Cu–Zn) (Querry 1985) can exhibit plasmonic properties as shown in their optical properties. According to

Fig. 1 The proposed biosensor design model

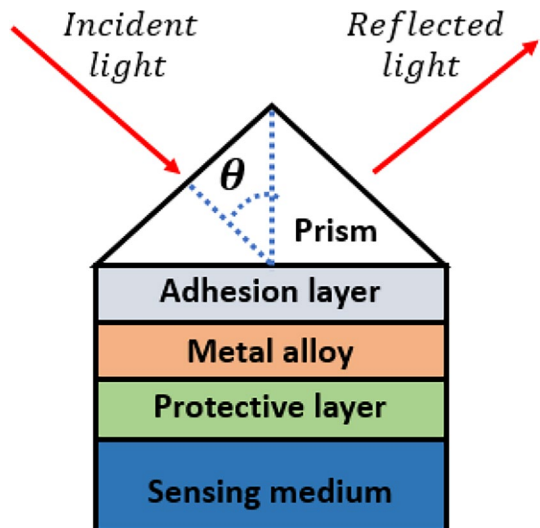


Table 1 Physical parameters of the proposed design model

Layer	Prism	Adhesion layer	Metal alloy	Protective layer	Sensing medium
Material	CaF ₂	ZnO	Au ₁₀ Ag ₉₀	Graphene	Water
Refractive index (at $\lambda = 633$ nm)	1.4329	1.98	0.10393 + 3.9578i	3.0 + 1.149i	1.333
Thickness (nm)	–	44	35	0.34	–

Papagiannouli et al. (2013), an Au–Ag alloy has enhanced oxidation and chemical stability due to the presence of Au atoms and produces stronger and narrower resonance curves due to the presence of Ag atoms. Rioux et al. (2014) compares effects of percentage ratios of Au versus Ag on optical properties of Au–Ag alloys. Different models are presented in the literature to determine complex refractive indices and dielectric functions of Au–Ag alloys with different composition ratios such as in Gaudry et al. (2001) and Rioux et al. (2014). The model by Rioux et al. (2014) is a modification of the famous Drude-Lorentz model (used for coinage metals). The modified model takes into account variations in free electron behavior in different composition ratios and also the actual metal band structures. In their work, Rioux et al. (2014) performed both theoretical and experimental studies to determine refractive indices and dielectric constants for different Au–Ag alloys (including Au₁₀Ag₉₀, Au₃₀Ag₇₀, Au₅₀Ag₅₀, Au₇₀Ag₃₀, and Au₉₀Ag₁₀) and their results are available in Polyanskiy, n.d.

Throughout this work, we consider only the optimal alloy thicknesses (d_{Alloy}) that allow maximum coupling between incident light and free electrons located at the metal alloy surface. This can be obtained by calculating the distribution of minimum values of the resonance reflectivity curve (R_{min}) which depends on θ_{SPR} and d_{Alloy} .

As previously discussed, ZnO possesses favorable optical and electrical characteristics. We add a ZnO adhesion layer ($n_{ZnO} = 1.98$) (Polyanskiy, n.d) between the prism and the metal alloy. Similarly, for ZnO, we select optimized thicknesses that give R_{min} corresponding to θ_{SPR} .

Taking into account the possibility that Au₁₀Ag₉₀ may still be somewhat susceptible to oxidation, we propose the addition of a graphene layer on top of the alloy. According to Zekriti (2021), graphene has a very low permeability which allows even a very thick graphene layer to protect Ag from oxidation without affecting resolution. Numerical analysis by Zekriti (2021) shows that graphene produces a sharp reflectivity curve compared to Au. Kumar et al. (2023) adds that there is a need to improve the adsorption of biomolecules to the SM as the attachment of some bio-sensing molecules to some sensor surfaces is a challenge. Furthermore, Song et al. (2010) and Homola (2003) discuss the excellent adsorption characteristics of graphene. This means graphene can serve as an absorption enhancement material, oxidation protection material, and sensitivity enhancement material. Piliarik and Homola (2009) mentions the visible range refractive index of graphene as

$$n_g = 3 + i(C/3)\lambda \quad (5)$$

where $C = 5.446 \mu\text{m}^{-1}$ and λ is the incident light wavelength. The thickness of graphene with L layers is $d_g = L \times 0.34$ nm.

For SM we use water ($n_w = 1.333$) (Polyanskiy, n.d). To decide sensitivity, we use a theoretical shift in the refractive index of the SM as $\Delta n_{SM} = 0.005$. Hossain et al. (2020) gives a

detailed study for determining Δn_{SM} after the addition of solutes and biomolecules with different concentrations.

2.3 Transfer matrix method (TMM)

Transfer Matrix Method (TMM) is a matrix-based analytical model used to describe the behavior and propagation of EM and acoustic waves through a multi-layer structure. According to Oliveira et al. (2019), TMM is derived from solutions of Maxwell's and Fresnel wave equations. Fresnel equations describe how light waves reflect, refract, and transmit at an interface between two media, while Maxwell's equations describe EM field continuity across different layers (Oliveira et al. 2019). We model our biosensor as a structure with 0 to N parallel layers in a 3D Cartesian plane system. Each layer j (where $j=0, \dots, N$) has refractive index n_j , dielectric constant ϵ_j , and thickness d_j . Each layer has its thickness increasing along the positive z -axis of the Cartesian plane, and this z -axis is normal to interface planes of the layers. We consider layer 0 as a prism and layer N as SM, thus, z increases from the prism to the SM. The wave vector in the positive z -direction, k_{zj} , is given by (Oliveira et al. 2019; Ong et al. 2006; Zekriti et al. 2015)

$$k_{zj} = \frac{2\pi}{\lambda} \sqrt{\epsilon_j - \epsilon_0 \sin^2(\theta)} \quad (6)$$

where λ and θ are wavelength and incidence angle of incident light respectively, while ϵ_0 and ϵ_j are dielectric constants of 0 th and j th layers respectively.

Fresnel transmission coefficients, t_{ij} , and Fresnel reflection coefficients, r_{ij} , are obtained as

$$r_{ij} = \left(\frac{k_{zi}}{\epsilon_i} - \frac{k_{zj}}{\epsilon_j} \right) / \left(\frac{k_{zi}}{\epsilon_i} + \frac{k_{zj}}{\epsilon_j} \right) \quad (7)$$

$$t_{ij} = 1 + r_{ij} \quad (8)$$

The above coefficients can be used to calculate a transition matrix between any two layers i and j , denoted M_{ij} , and a propagation matrix in a medium j , denoted P_j , as,

$$M_{ij} = \frac{1}{t_{ij}} \begin{pmatrix} 1 & r_{ij} \\ r_{ij} & 1 \end{pmatrix} \quad (9)$$

$$P_j = \begin{pmatrix} e^{ik_{zj}d_j} & 0 \\ 0 & e^{-ik_{zj}d_j} \end{pmatrix} \quad (10)$$

Given fields of the incident and reflected light at layer 0 as $H_{o,i}$ and $H_{o,r}$ respectively, and that field of transmitted light at layer N is $H_{N,t}$, a relation between these fields can be given by a product of transition and propagation matrices, M_{ij} , and P_j , respectively, as

$$\begin{pmatrix} H_{o,r} \\ H_{o,i} \end{pmatrix} = M_{0,1} P_1 M_{1,2} P_2 \dots P_{N-1} M_{N-1,N} \begin{pmatrix} 0 \\ H_{N,t} \end{pmatrix} = S_{0,N} \begin{pmatrix} 0 \\ H_{N,t} \end{pmatrix} \quad (11)$$

where $S_{0,N}$ is a 2×2 matrix,

$$S_{0,N} = \begin{pmatrix} S_{11} & S_{12} \\ S_{21} & S_{22} \end{pmatrix} \quad (12)$$

From Eqs. (11) and (12), we get reflection ($r_{0,N}$) and transmission ($t_{0,N}$) coefficients of the whole multi-layer structure as,

$$r_{0,N} = \frac{H_{0,r}}{H_{0,i}} = \frac{S_{12}}{S_{22}} \quad (13)$$

$$t_{0,N} = \frac{H_{N,t}}{H_{0,i}} = \frac{1}{S_{22}} \quad (14)$$

2.4 Performance metrics

Different metrics are used to analyze the performance of an SPR-based biosensor. To begin with, reflectivity and transmissivity, when light strikes the surface of the biosensor, part of it is transmitted through the biosensor to cause the SPR phenomenon, while a portion is reflected. The ratio of reflected light versus incident light is called reflectivity (R), whereas the ratio of transmitted light versus incident light is called transmissivity (T), considering an N-layer biosensor, reflectivity and transmissivity are obtained from reflection and transmission coefficients (Eqs. (13) and (14), respectively) as, (Oliveira et al. 2019; Ong et al. 2006; Zekriti et al. 2015)

$$R = |r_{0,N}|^2 \quad (15)$$

$$T = |t_{0,N}|^2 \quad (16)$$

Sensitivity (S_y) is the ratio of the shift in resonance angle ($\Delta\theta_{SPR}$) to the change in the refractive index (Δn) of the SM given as, (Homola 2006; Tetyana et al. 2021)

$$S_y = \frac{\Delta\theta_{SPR}}{\Delta n} \quad (17)$$

In an N-layer biosensor, the Field Enhancement (FE) factor gives the ratio of the intensity of electric field ($|E|^2$) or magnetic field ($|H|^2$) at the sensing interface ($N-1/N$), to the intensity at the first interface ($0/1$). Electric and magnetic field values are related to the transmission coefficient (t) of the biosensor by the ratio of real values of dielectric constants of layer 0 and layer N (ϵ_0 and ϵ_N respectively), as follows, (Kumar et al. 2018; Ong et al. 2006)

$$FE = \left| \frac{E(N/N-1)}{E(0/1)} \right|^2 = \frac{\epsilon_0}{\epsilon_N} \left| \frac{H_y(N/N-1)}{H_y(0/1)} \right|^2 = \frac{\epsilon_0}{\epsilon_N} |t|^2 \quad (18)$$

Full Width at Half Maximum (FWHM) shows the width of the reflectivity dip at a position where reflectivity is half of its maximum value. A smaller FWHM helps achieve better sensitivity and resolution.

Detection Accuracy (DA) is the inverse value of FWHM. A higher DA signifies a narrower FWHM. (Maharana et al. 2015).

$$DA = 1/FWHM \quad (19)$$

In SPR biosensors, Signal to Noise Ratio (SNR) is given by, (Akib et al. 2021; Kumar et al. 2020)

$$SNR = \frac{\Delta\theta_{SPR}}{FWHM} \quad (20)$$

Figure of merit (FoM) is a measure used to quantify the performance of an SPR biosensor. FoM is represented as the ratio of sensitivity to FWHM, (Akib et al. 2021)

$$FOM = \frac{S_y}{FWHM} \quad (21)$$

Lastly, Quality Factor (QF) is another measure used to quantify the performance of SPR biosensors and is dependent on SNR and sensitivity as follows, (Akib et al. 2021).

$$QF = SNR \times S_y \quad (22)$$

3 Results and discussion

In this section, we present simulation results showing the performance of the proposed designs.

3.1 Performance and selection of glass prism

Different glass prisms from the literature (CaF₂, BK7, SF10, and LASF9) were considered to check performance with Au–Ag alloy in a conventional configuration of Prism/Au₁₀Ag₉₀/SM. For each prism, we present performance results obtained using an optimized thickness of the alloy. Figure 2a shows reflectivity curves for the different prisms, whereas Fig. 2b shows variations in sensitivity and FoM against the refractive indices of the prisms. Table 2 presents all simulation results for prism selection.

To begin with, Fig. 2a shows that as the refractive index of the glass prism (n_p) increases, the resonance angle (θ_{SPR}) shifts to smaller values. This trend agrees with literature such as (Karki et al. 2022; Uniyal et al. 2022) who also found that a lower index prism gives a larger resonance angle. In general, the choice of prism helps determine the resonance angle. Secondly, as the refractive index of the glass prism (n_p) increases, FWHM becomes smaller. We observe larger FWHM in configuration with CaF₂ ($n_{CaF_2} = 1.4329$). FWHM tends to decrease as we shift towards LASF9 ($n_{LASF9} = 1.8449$). Similarly, Karki et al. (2022); Kumar et al. (2018); Uniyal et al. (2022) also show that high refractive index prisms produce narrow and sharp resonance curves.

From Fig. 2b, we observe that as the refractive index increases, sensitivity also decreases causing a decrease in FoM. The decrease in sensitivity is due to a decrease in resonance shift over the different glass prisms. From Table 2 results, we also observe a decrease in the optimum alloy thicknesses. From these results, we therefore select CaF₂ because it has

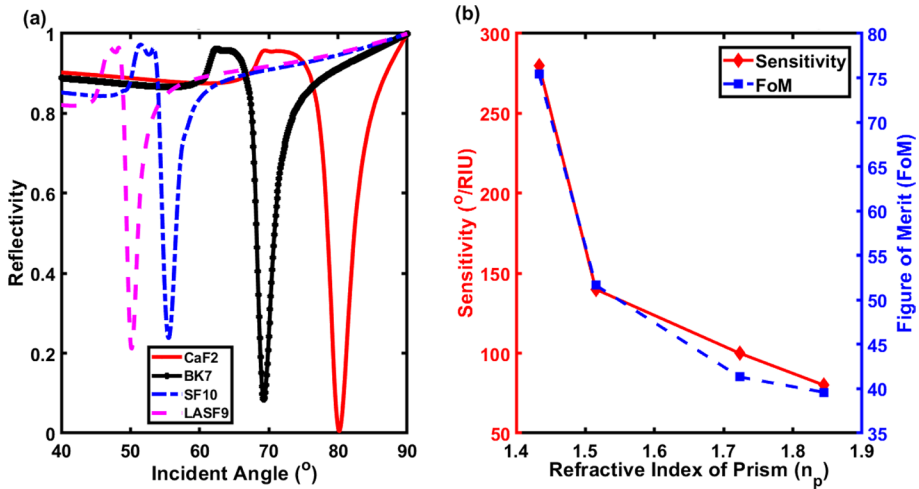


Fig. 2 **a** Reflectivity curves for different glass prisms with $Au_{10}Ag_{90}$ alloy. **b** Variations in sensitivity and FoM over different prism refractive indices

Table 2 Performance of different glass prisms with $Au_{10}Ag_{90}$ alloy of different optimized thicknesses (d_{Alloy}).

Note: Refractive indices of prisms obtained from (Moznuzzaman et al. 2021; Polyanskiy, n.d)

Prism (n_p)	d_{Alloy} (nm)	θ_{SPR} (°)	θ_{SPR2} (°)	$\Delta\theta_{SPR}$ (°)	FWHM (°)	S_y (°/RIU))	FoM (/RIU)
CaF ₂ (1.4329)	47	80.3	81.7	1.4	3.71	280	75.47
BK7 (1.5151)	45	69.4	70.1	0.7	2.71	140	51.66
SF10 (1.7230)	41	55.6	56.1	0.5	2.42	100	41.32
LASF9 (1.8449)	39	50.3	50.7	0.4	2.02	80	39.60

better performance in terms of: larger resonance shift ($\Delta\theta_{SPR} = 1.4^\circ$), highest sensitivity ($S_y = 280^\circ/RIU$) and largest figure of merit ($FoM = 75.47/RIU$).

3.2 Performance and selection of Au–Ag alloy

As previously discussed, the optical characteristics of Au–Ag alloys vary according to their composition ratios. Here, we consider the alloys: $Au_{10}Ag_{90}$, $Au_{30}Ag_{70}$, $Au_{50}Ag_{50}$, $Au_{70}Ag_{30}$, and $Au_{90}Ag_{10}$. Note that in Au_xAg_{100-x} notation, x and $100-x$ represent composition percentages of Au and Ag respectively. Figure 3 illustrates the real permittivity values ($Re(\epsilon_m)$) and imaginary permittivity values ($Im(\epsilon_m)$) for the Au–Ag alloys at 633 nm as the percentage portion of Ag increases while the percentage portion of Au decreases.

We use the configuration $CaF_2/Au_xAg_{100-x}/SM$ with varying alloy compositions and optimized alloy thicknesses to observe performance of the different alloys. Figure 4 shows reflectivity and field enhancement (FE) graphs for the different Au–Ag alloys. This figure shows that, as the composition percentage of Au and Ag (henceforth denoted Au% and Ag% respectively) varies, they affect the performance of our structure. According to Alisawi et al. (2013), adjusting the percentage ratios of composition elements influences an alloy’s optical and electrochemical properties.

Fig. 3 Permittivity of Au–Ag alloys at 633 nm with increasing portion of Ag

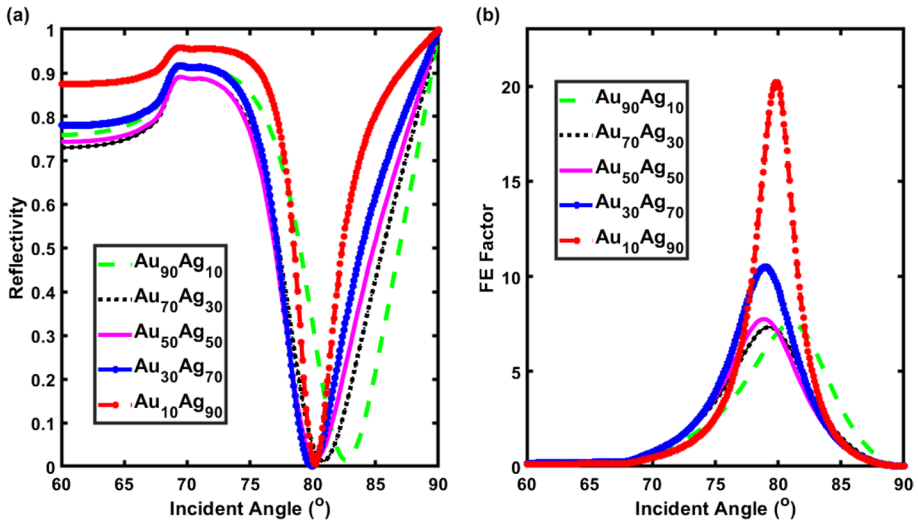
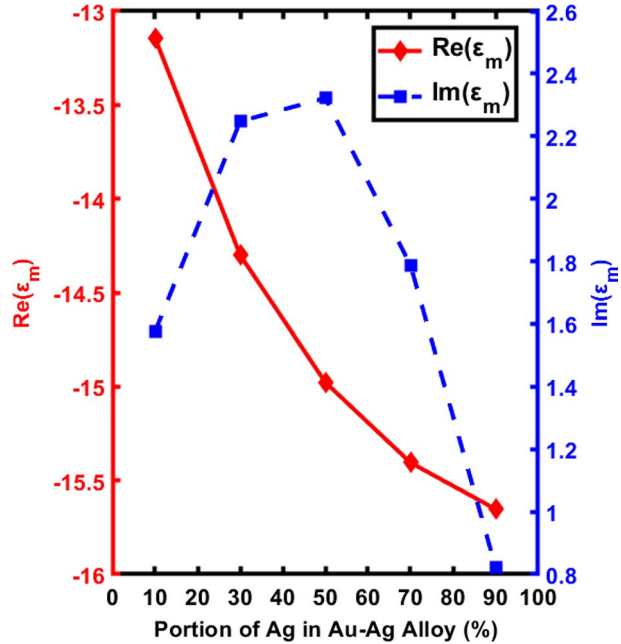


Fig. 4 **a** Reflectivity, and **b** Field Enhancement (FE) of different Au–Ag alloys with optimized alloy thicknesses

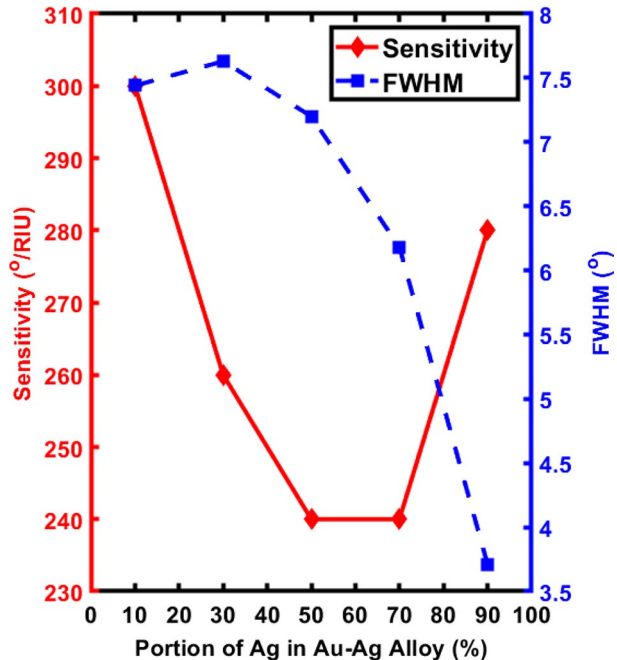
From Fig. 4a we see that while Ag% increases, the resonance angle slowly shifts to lower values. Au₉₀Ag₁₀ has a resonance at 81.8°, while Au₁₀Ag₉₀ has a resonance at 80.3°. Homola et al. (1999) states that pure Au has a larger resonance angle compared to pure Ag. This is because of variations in the optical properties of these metals. In terms of alloys, as the composition of one metal increases, the alloy tends to have optical behavior closer

to that of the dominant metal. Despite this, our results show resonance angles are within a smaller range since resonance angles are usually dependent on prism and SM, which in this case are the same.

Figure 4b shows how Ag% affects the FE of the structure. We observe that this FE depends on the amount of Ag in the alloy, with significant differences for high Ag proportions (from 70% to 90%) and low Ag proportions (from 10% to 50%). The effect of the permittivity was discussed in depth by Raether (1988) who demonstrated that the FE in the Kretschmann configuration is proportional to $|Re(\epsilon_m)|^2/Im(\epsilon_m)$. This FE follows approximately the same trends as the real and imaginary parts of the alloy's permittivity (see Fig. 3). In fact, for lower proportions of Ag, $|Re(\epsilon_m)|$ and $Im(\epsilon_m)$ increase with an increase in Ag%. This proportionality of increase in both $|Re(\epsilon_m)|$ and $Im(\epsilon_m)$ compensates the effect of these terms on each other which makes the FE relatively stable at lower Ag% values. However, for higher proportions of silver, $|Re(\epsilon_m)|$ increases while $Im(\epsilon_m)$ decreases, hence increasing the FE at the metal/SM interface. This is why we observe higher FE results in structures with Au₇₀Ag₃₀, and Au₉₀Ag₁₀.

Figure 5 shows variations in sensitivity and FWHM as Ag% increases. This figure shows that all alloys considered here give better sensitivity. The sensitivity behavior of an SPR sensor to bulk refractive index change is discussed in depth by Homola (2006) and calculated by using perturbation theory. From this work, it is observed that sensitivity depends on the metal's permittivity, resonance angle location, and metal thickness. Higher resonance angle and optimized metal thickness lead to better sensitivity. Based on this and as follows from Fig. 5, we observe that as Ag% goes from 10% to 70%, sensitivity decreases significantly. This can be attributed mainly to the change in the permittivity causing resonance angle shift to lower angles, while the optimal thicknesses are almost the same. However, for Ag% equal to 90%, sensitivity reaches 280°/RIU. This is because the optimal alloy thickness in this case (47 nm) leading to better coupling efficiency is greater

Fig. 5 Variations in sensitivity and FWHM with increasing portion of Ag in Au–Ag alloys



than the optimal thicknesses corresponding to the other Ag proportions. In addition, the use of a prism with a low refractive index is another factor that leads to these enhanced sensitivity values. In comparison, $\text{Au}_{90}\text{Ag}_{10}$ has the highest sensitivity ($300^\circ/\text{RIU}$) followed by $\text{Au}_{10}\text{Ag}_{90}$ ($280^\circ/\text{RIU}$).

Furthermore, Fig. 5 shows that an increase in Ag% causes a decrease in FWHM. $\text{Au}_{90}\text{Ag}_{10}$ (with Ag% of 10%) has the largest FWHM of 7.44° , while $\text{Au}_{10}\text{Ag}_{90}$ (with Ag% of 90%) exhibits the lowest FWHM of 3.71° . As previously discussed, pure Ag produces smaller FWHM and better sensitivity than Au. Thus, it is reasonable to observe that an increase in the Ag portion in the alloys causes a decrease in the FWHM. Considering all sensing performance results, $\text{Au}_{10}\text{Ag}_{90}$ gives good sensitivity ($280^\circ/\text{RIU}$), the smallest FWHM (3.71°), the highest FoM ($75.47/\text{RIU}$), and the best FE factor (20.2). Table 3 shows all performance results for the different Au–Ag alloys.

3.3 Performance analysis while using adhesion and protective layers

We study the impact of each proposed additional layer (ZnO and graphene) by using four proposed design structures shown in Fig. 6.

Structure 1 has $\text{Au}_{10}\text{Ag}_{90}$ alloy in a conventional Kretschmann configuration with CaF_2 prism and water as SM. This design is modified by the addition of graphene as a protective and adsorption layer to give structure 2, and the addition of ZnO as an adhesion layer to give structure 3. Lastly, structure 4 consists addition of both ZnO and graphene. Optimized thicknesses for these layers are presented in Table 4.

Figure 7 shows graphs of reflectivity and FE for the proposed structures. These graphs show that the use of alloy and CaF_2 prism in design 1 produces resonance at 80.3° , with FWHM of 3.71° and FE of 20.2. With the addition of a graphene layer on top of the alloy (making structure 2), the resonance position changes to 81.0° while FWHM increases to 4.25° and FE decreases to 14.6. The high refractive index of graphene allows it to alter the propagation of surface plasmons thus shifting the resonance angle. In addition, graphene provides a conductive and high surface area for efficient binding of biomolecules, hence improving sensitivity. Despite this, increasing the number of graphene layers increases absorption properties in the structure causing further drop in FE and further widening of FWHM. Due to this, we limit our selection to one layer of graphene.

Results of structure 3 show that the addition of a ZnO layer between the prism and alloy changes the resonance position to 81.3° . Furthermore, FE decreases from 20.2 to 17.3. This is due to the high refractive index property of ZnO as well. In addition, ZnO widens FWHM from 3.71° to 4.8° . In structure 4, we observe the effects of adding both the ZnO layer and the graphene layer in the same biosensor design. Results show a significant change in resonance position to 82.0° , while FWHM widens further to 5.64° . The increase in sensing layers causes a drop in the FE factor to 12.6.

It is worth noting that in structures 1 and 2 the excitation of SPR is ensured via the total internal reflection that light undergoes in the prism. However, in structures 3 and 4 the generation of the SPR at the metal alloy surface is performed after passing through the ZnO layer where an amount of light remains confined and back-coupled to radiation loss. Hence, the use of ZnO gives lower FE in comparison with the former case. On the other hand, the effect of graphene that was observed in structures 2 and 4 is similar in both cases.

We also draw the attention of the readers that the thicknesses in each design are selected after performing several simulations in such a way that a maximum coupling between

Table 3 Performance of different Au–Ag alloys with different optimized thicknesses

Alloy	d_{Alloy} (nm)	$\theta_{\text{SPR}}(^{\circ})$	$\theta_{\text{SPR}2} (^{\circ})$	$\Delta\theta_{\text{SPR}} (^{\circ})$	FWHM ($^{\circ}$)	DA ($^{\circ}$)	Sy ($^{\circ}$ /RIU)	FoM (/RIU)	SNR	QF (/RIU)
Au ₁₀ Ag ₉₀	47	80.3	81.7	1.4	3.71	0.27	280	75.47	0.38	105.66
Au ₃₀ Ag ₇₀	41	80.0	81.2	1.2	6.18	0.16	240	38.83	0.19	46.60
Au ₅₀ Ag ₅₀	40	80.3	81.5	1.2	7.20	0.14	240	33.33	0.17	40.00
Au ₇₀ Ag ₃₀	40	80.9	82.2	1.3	7.63	0.13	260	34.08	0.17	44.30
Au ₉₀ Ag ₁₀	42	82.8	84.3	1.5	7.44	0.13	300	40.32	0.20	60.48

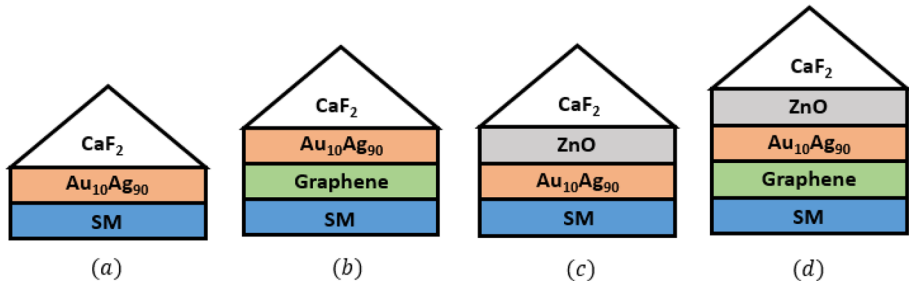


Fig. 6 Proposed designs: **a** structure 1, **b** structure 2, **c** structure 3, and **d** structure 4

Table 4 Proposed design structures with optimized layer thicknesses

Design	Configuration
1	CaF ₂ /Au ₁₀ Ag ₉₀ (47 nm)/SM
2	CaF ₂ /Au ₁₀ Ag ₉₀ (49 nm)/Graphene (0.34 nm)/SM
3	CaF ₂ /ZnO (44 nm)/Au ₁₀ Ag ₉₀ (35 nm)/SM
4	CaF ₂ /ZnO (44 nm)/Au ₁₀ Ag ₉₀ (35 nm)/Graphene (0.34 nm)/SM

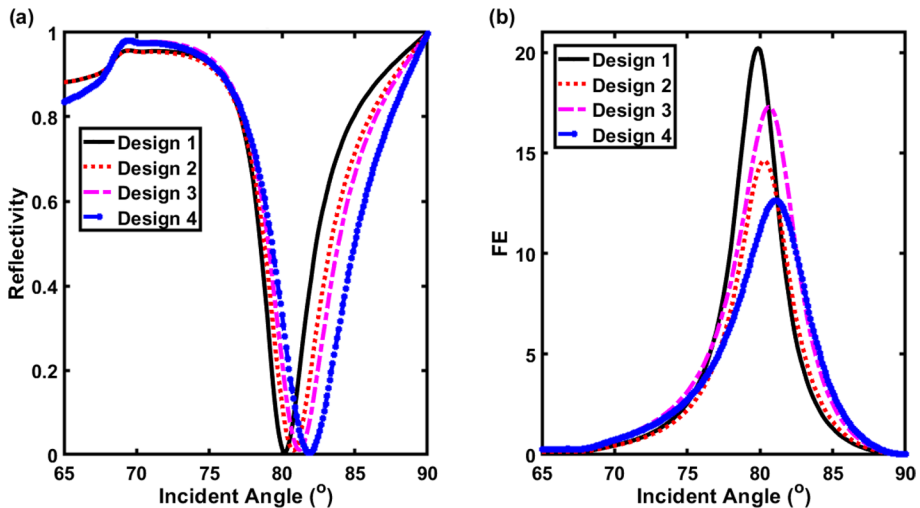


Fig. 7 **a** Reflectivity, and **b** FE graphs of the proposed structures

incident light and free electrons on the alloy surface can be obtained. This is the reason why the R_{\min} of the four designs reaches zero.

Figure 8 shows the reflectivity curves of the proposed structures and their corresponding curve shifts due to a change in the SM's refractive index of $\Delta n_{\text{SM}} = 0.005$. Magnitudes of resonance angle shifts and corresponding sensitivity values are also indicated. From our results, structure 1 produces the lowest angular shift of 1.4° corresponding to sensitivity of $280^\circ/\text{RIU}$. The addition of different layers improves this sensitivity such as the addition of

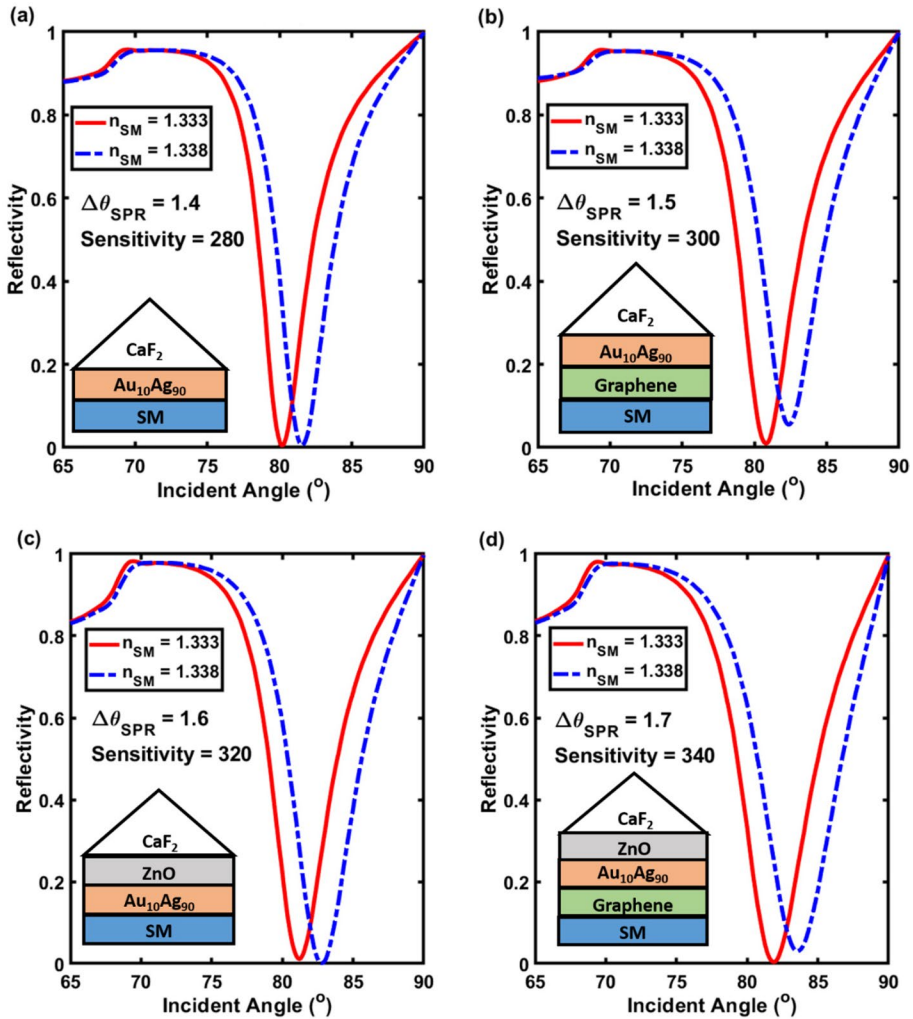


Fig. 8 Reflectivity shift due to change in refractive index of the sensing medium ($\Delta n_{SM} = 0.005$) for the proposed structures: **a** structure 1, **b** structure 2, **c** structure 3, and **d** structure 4

graphene producing $300^\circ/\text{RIU}$ (structure 2) and the addition of ZnO producing $320^\circ/\text{RIU}$ (structure 3). Finally, the addition of ZnO and graphene in the same design produces a sensitivity of $340^\circ/\text{RIU}$ (structure 4). These high sensitivity values are due to the different layers including the use of low index CaF_2 prism and the alloy.

Table 5 shows all simulation results of the proposed structures. By comparison, structure 1 has better FoM ($75.47/\text{RIU}$), QF ($105.88/\text{RIU}$), and FE (20.2); but a sensitivity of $280^\circ/\text{RIU}$. Structure 4 has the highest sensitivity ($340^\circ/\text{RIU}$); but the lowest FE factor (12.6) due to the additional layers. Despite reducing FE, we emphasize the importance of graphene and ZnO on the biosensor.

As previously discussed, the advantage of using pure Ag in SPR biosensors is that it possesses a narrow FWHM, and it produces better sensitivity; but Ag has poor chemical stability. Since then, bimetallic configurations have attracted a lot of interest as a good

Table 5 Performance of the proposed design structures

Design	$\theta_{\text{SPR}}(^{\circ})$	$\theta_{\text{SPR}2} (^{\circ})$	$\Delta\theta_{\text{SPR}} (^{\circ})$	FWHM ($^{\circ}$)	DA ($^{\circ}$)	Sy ($^{\circ}$ /RIU)	FoM (/RIU)	SNR	QF (/RIU)	FE
1	80.3	81.7	1.4	3.71	0.27	280	75.47	0.38	105.66	20.2
2	81.0	82.5	1.5	4.25	0.24	300	70.59	0.35	105.88	14.6
3	81.3	82.9	1.6	4.8	0.21	320	66.67	0.33	106.67	17.3
4	82.0	83.7	1.7	5.64	0.18	340	60.28	0.30	102.48	12.6

approach to improving the stability of Ag-based biosensors. Meanwhile, the use of Au as a protective layer can, at the same time, enhance the sensitivity and ensure higher stability. Now, in this study, we have proposed the use of Au–Ag alloys as the new approach to improve the chemical stability of Ag which is proportional to the amount of Au in the alloy. After performing several simulations to compare the effect of Au proportion on the sensitivity of the sensor, we judge that the use of only 10% of Au gives the best performance characteristics concerning higher proportions. In such a situation, the chemical stability will not be enhanced significantly. This is the reason why in our final proposed design we use graphene as a protective layer to ensure better stability. Similarly and as previously discussed, the interaction between the prism and the alloy is enhanced by the use of ZnO which has been shown to improve sensitivity as well. In this consideration, we therefore propose structure 4 as the best design.

3.4 Electric field distribution profile

The absolute electric field intensity ($|E|^2$) profile demonstrates the behavior of the electric field along each layer in a multilayer biosensor structure. In this work, we use Lumerical FDTD software to obtain field profiles. Figure 9 shows the obtained results at corresponding resonance angles plotted against normal distance (z) for the proposed structures. As follows from the figure, we observe an enhanced electric field at the sensing interface of each structure, which is important for high-precision sensing applications. Structure 1 exhibits the highest value of the maximum field followed by structure 3. This can be explained by the presence of ZnO in structure 3 which leads to a back-coupled radiation loss. On the other hand, the addition of graphene reduces the field intensity at the sensing interface, which is due mainly to the absorption of light by graphene.

The penetration depth (PD) of the field in the SM is another parameter to be taken into account in the estimation of the sensing performance of any SPR sensor. PD can be defined as the distance at which the field decays to $1/e$ (or approximately 37%) of its maximum value (Homola 2003). From our results, we find that the PD of the field is not significantly

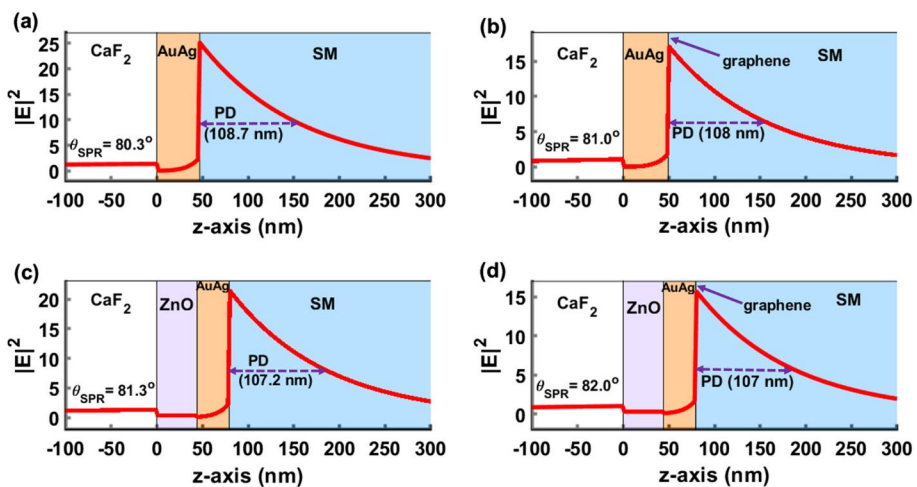


Fig. 9 Electric field intensity distribution profiles of the proposed structures: **a** structure 1, **b** structure 2, **c** structure 3, and **d** structure 4

affected by the inclusion of ZnO, graphene, or both of them. This is because in this study we considered the use of only one layer of graphene with a thickness of 0.34 nm and the use of the ZnO layer is located between the prism and the metal alloy surface which makes it far from the metal/SM interface.

Figure 10 presents the field profiles as a function of incidence angle and normal distance (z). In each plot, we observe the surface plasmon mode occurring at the corresponding resonance angles. Furthermore, the PD and TIR angle are also shown. As previously discussed, θ_{TIR} is dependent on the prism and dielectric material properties. According to Eq. (3), and considering $\epsilon_d = \epsilon_{SM}$, we obtain $\theta_{TIR} = 68.5^\circ$ for all structures. In our results, we observe resonance at angles above the TIR angle.

3.5 Comparison with other theoretical results

In this work, we have presented a theoretical study of different SPR biosensor designs from which we have recommended one final design structure. The main objective of this work is to present a high-performing structure, especially with high sensitivity. High sensitivity has a direct effect on other biosensor performance metrics like specificity, detection limit, dynamic range, and response time. In this regard, in Table 6 we compare the sensitivity

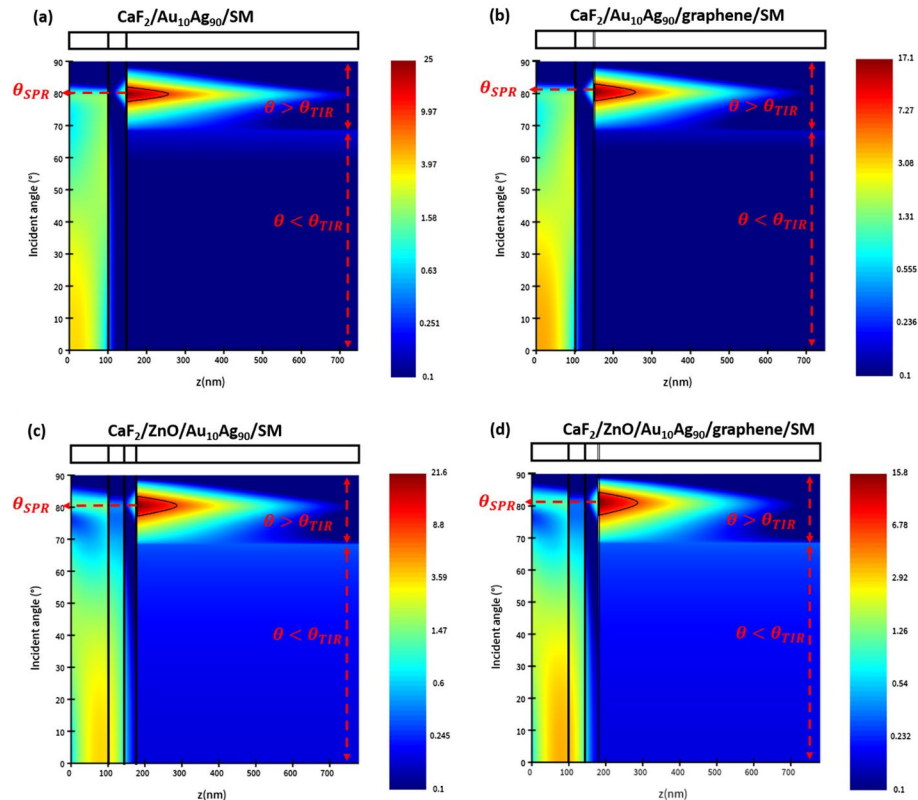


Fig. 10 Electric field intensity distribution profiles of the proposed structures as a function of incidence angle and normal distance (z): **a** structure 1, **b** structure 2, **c** structure 3, and **d** structure 4

Table 6 Comparison in sensitivity of the proposed structure versus other structures in literature

References of structure	Configuration	Sy (°/RIU)
Kumar et al. (2023)	BK7/MgO/Ag/BP/SM	234
Singh et al. (2021)	CaF ₂ /ZnO/Au/BlueP-MoS ₂ /SM	235
Kumar et al. (2018)	BK7/ ZnO/Ag/Au/graphene/SM	76
Kumar et al. (2020)	BK7/ZnO/Ag/BaTiO ₃ /graphene/SM	157
Basak et al. (2020)	SF10/ZnO/Au/WSe ₂ /BP/SM	102
Mostufa et al. (2022)	BK7/ TiO ₂ /Au/graphene /SM	293
Raikwar et al. (2021)	BK7/TiO ₂ /Au/MXene/Sb/SM	224.26
Singh et al. (2023)	CaF ₂ /Ag/ Fe ₂ O ₃ /Ni/Sb/SM	204
Karki et al. (2022)	BK7/Ag/ZnS/graphene/SM	292.8
Dai et al. (2019)	BK7/Ag/SnSe/SM	178
Gan et al. (2019)	BK7/Ag/franckeite/SM	188
Jia et al. (2022)	BK7/Au/GeS/SM	260
Proposed	CaF ₂ /ZnO/Au ₁₀ Ag ₉₀ /graphene/SM	340

performance of our proposed design (structure 4) to different theoretical design structures provided in the literature.

According to these results, it is evident that our proposed structure exhibits the highest sensitivity (340°/RIU). High sensitivity is a very crucial parameter in different applications especially the detection of tiny cancer bio-markers. High sensitivity allows observation of very small concentrations of these bio-markers in body fluids which enables early diagnosis thus allowing early cancer treatment intervention.

4 Conclusion

Various materials and methods have been suggested to improve the performance of SPR-based biosensors. In this work, we have presented sensitivity and performance enhancement using a low refractive index CaF₂ glass prism, a gold–silver alloy (Au₁₀Ag₉₀), and additional layers in terms of ZnO and 2D graphene. Apart from supporting SPR and enhancing sensitivity, the use of ZnO is to improve adhesion between the prism and alloy, while graphene promises better biomolecule adhesion and improved biostability. Our final proposed structure, having the configuration CaF₂/ZnO/Au₁₀Ag₉₀/graphene/SM, has the highest sensitivity (340°/RIU), high figure of merit (60.28/RIU), and a high quality factor (102.48/RIU). Sensitivity directly affects other performance metrics such as specificity, detection limit, dynamic range, and response time. Therefore, the high sensitivity of our proposed biosensor makes it suitable for the detection of tiny cancer bio-markers in body fluids. These markers can be detected even in very small concentrations, enabling early diagnosis and early medical interventions. Practical steps to realize the biosensor chip in real life have also been presented. Further research can focus on increasing field enhancement and surface plasmon penetration depth.

Acknowledgements The authors are thankful to the Euro-Mediterranean University of Fes (UEMF) and the African Scientific Research and Innovation Council (ASRIC) of the African Union (AU) for supporting this research work.

Author contributions Innocent Kadaleka Phiri was responsible for conceptualization, software, formal analysis, and writing of the original draft. Prof. Mohssin Zekriti was responsible for conceptualization, validation, writing—review & editing, and supervision.

Funding There is no funding to declare.

Data availability No datasets were generated or analysed during the current study.

Declarations

Conflict of interest The authors declare that they have no competing interests.

Permissions All the included figures, tables, or text passages that have already been published elsewhere have obtained permission from the copyright owner(s) for both the print and online format.

References

- Akib, T.B.A., Mou, S.F., Rahman, Md.M., Rana, Md.M., Islam, Md.R., Mehedi, I.M., Mahmud, M.A.P., Kouzani, A.Z.: Design and numerical analysis of a graphene-coated SPR biosensor for rapid detection of the novel coronavirus. *Sensors* **21**(10), 3491 (2021). <https://doi.org/10.3390/s21103491>
- Alissawi, N., Zaporotchenko, V., Strunskus, T., Kocabas, I., Chakravadhanula, V.S.K., Kienle, L., Garbe-Schönberg, D., Faupel, F.: Effect of gold alloying on stability of silver nanoparticles and control of silver ion release from vapor-deposited Ag–Au/polytetrafluoroethylene nanocomposites. *Gold Bull.* **46**(1), 3–11 (2013). <https://doi.org/10.1007/s13404-012-0073-6>
- Barnes, W.L.: Surface plasmon–polariton length scales: a route to sub-wavelength optics. *J. Opt. a: Pure Appl. Opt.* **8**(4), S87–S93 (2006). <https://doi.org/10.1088/1464-4258/8/4/S06>
- Barnes, W.L., Dereux, A., Ebbesen, T.W.: Surface plasmon subwavelength optics. *Nature* **424**(6950), 824–830 (2003). <https://doi.org/10.1038/nature01937>
- Basak, C., Hosain, Md.K., Sazzad, A.A.: Design and simulation of a high sensitive surface plasmon resonance biosensor for detection of biomolecules. *Sens. Imaging* **21**(1), 2 (2020). <https://doi.org/10.1007/s11220-019-0267-6>
- Cortie, M.B., Arnold, M.D., Keast, V.J.: The quest for zero loss: unconventional materials for plasmonics. *Adv. Mater.* **32**(18), 1904532 (2020). <https://doi.org/10.1002/adma.201904532>
- Dai, X., Liang, Y., Zhao, Y., Gan, S., Jia, Y., Xiang, Y.: Sensitivity enhancement of a surface plasmon resonance with tin selenide (SnSe) Allotropes. *Sensors* **19**(1), 173 (2019). <https://doi.org/10.3390/s19010173>
- Gan, S., Zhao, Y., Dai, X., Xiang, Y.: Sensitivity enhancement of surface plasmon resonance sensors with 2D franckeite nanosheets. *Res. Phys.* **13**, 102320 (2019). <https://doi.org/10.1016/j.rinp.2019.102320>
- Gaudry, M., Lermé, J., Cottancin, E., Pellarin, M., Vialle, J.-L., Broyer, M., Prével, B., Treilleux, M., Mélinon, P.: Optical properties of (AuxAg_{1-x})_n clusters embedded in alumina: evolution with size and stoichiometry. *Phys. Rev. B* **64**(8), 085407 (2001). <https://doi.org/10.1103/PhysRevB.64.085407>
- Gray, S.K.: Theory and modeling of plasmonic structures. *J. Phys. Chem. C* **117**(5), 1983–1994 (2013). <https://doi.org/10.1021/jp309664c>
- Homola, J.: Present and future of surface plasmon resonance biosensors. *Anal. Bioanal. Chem.* **377**(3), 528–539 (2003). <https://doi.org/10.1007/s00216-003-2101-0>
- Homola, J. (Ed.): *Surface Plasmon Resonance Based Sensors*, Vol. 4. Springer. (2006). <https://doi.org/10.1007/b100321>
- Homola, J., Yee, S.S., Gauglitz, G.: Surface plasmon resonance sensors: review. *Sens. Actuators, B Chem.* **54**(1–2), 3–15 (1999). [https://doi.org/10.1016/S0925-4005\(98\)00321-9](https://doi.org/10.1016/S0925-4005(98)00321-9)
- Hossain, Md.B., Islam, Md.M., Abdulrazak, L.F., Rana, Md.M., Akib, T.B.A., Hassan, M.: Graphene-coated optical fiber SPR biosensor for BRCA1 and BRCA2 breast cancer biomarker detection: a numerical design-based analysis. *Photonics Sens.* **10**(1), 67–79 (2020). <https://doi.org/10.1007/s13320-019-0556-7>
- Jia, Y., Liao, Y., Cai, H., Lopomo, F., Jia, Y., Liao, Y., Cai, H.: Sensitivity Improvement of Surface Plasmon Resonance Biosensors with GeS-Metal Layers. (2022). <https://doi.org/10.3390/electronics11030332>
- Karki, B., Uniyal, A., Chauhan, B., Pal, A.: Sensitivity enhancement of a graphene, zinc sulfide-based surface plasmon resonance biosensor with an Ag metal configuration in the visible region. *J. Comput. Electron.* **21**(2), 445–452 (2022). <https://doi.org/10.1007/s10825-022-01854-4>

- Knoll, W.: Interfaces and thin films as seen by bound electromagnetic waves. *Annu. Rev. Phys. Chem.* **49**(1), 569–638 (1998). <https://doi.org/10.1146/annurev.physchem.49.1.569>
- Kretschmann, E., Raether, H.: Notizen: radiative decay of non radiative surface plasmons excited by light. *Zeitschrift Für Naturforschung A* **23**(12), 2135–2136 (1968). <https://doi.org/10.1515/zna-1968-1247>
- Kumar, A., Yadav, A.K., Kushwaha, A.S., Srivastava, S.K.: A comparative study among WS₂, MoS₂ and graphene based surface plasmon resonance (SPR) sensor. *Sens. Actuators Rep.* **2**(1), 100015 (2020). <https://doi.org/10.1016/J.SNR.2020.100015>
- Kumar, R., Kushwaha, A.S., Srivastava, M., Mishra, H., Srivastava, S.K.: Enhancement in sensitivity of graphene-based zinc oxide assisted bimetallic surface plasmon resonance (SPR) biosensor. *Appl. Phys. A* **124**(3), 235 (2018). <https://doi.org/10.1007/s00339-018-1606-5>
- Kumar, S., Yadav, A., Malomed, B.A.: High performance surface plasmon resonance based sensor using black phosphorus and magnesium oxide adhesion layer. *Front. Mater.* **10**, 1131412 (2023). <https://doi.org/10.3389/fmats.2023.1131412>
- Mafazi, I. R., Yuliarto, B., Gumilar, G., Nur, L. O.: Modeling and optimization of surface plasmon resonance sensors using metamaterials. In: 2022 11th Electrical Power, Electronics, Communications, Controls and Informatics Seminar (EECCIS), pp. 211–214. (2022). <https://doi.org/10.1109/EECCI554468.2022.9902906>
- Maharana, P.K., Jha, R., Padhy, P.: On the electric field enhancement and performance of SPR gas sensor based on graphene for visible and near infrared. *Sens. Actuators b: Chem.* **207**(Part A), 117–122 (2015). <https://doi.org/10.1016/J.SNB.2014.10.006>
- Miyazaki, C. M., Shimizu, F. M., Ferreira, M.: Surface plasmon resonance (SPR) for sensors and biosensors. In: *Nanocharacterization Techniques*, pp. 183–200. Elsevier. (2017). <https://doi.org/10.1016/B978-0-323-49778-7.00006-0>
- Mostufa, S., Akib, T.B.A., Rana, M.M., Islam, M.R.: Highly sensitive TiO₂/Au/graphene layer-based surface plasmon resonance biosensor for cancer detection. *Biosensors* **12**(8), 603 (2022). <https://doi.org/10.3390/bios12080603>
- Moznuzzaman, Md., Islam, Md.R., Khan, I.: Effect of layer thickness variation on sensitivity: an SPR based sensor for formalin detection. *Sens. Bio-Sens. Res.* **32**, 100419 (2021). <https://doi.org/10.1016/j.sbsr.2021.100419>
- Mudgal, N., Saharia, A., Choure, K.K., Agarwal, A., Singh, G.: Sensitivity enhancement with anti-reflection coating of silicon nitride (Si₃N₄) layer in silver-based surface plasmon resonance (SPR) sensor for sensing of DNA hybridization. *Appl. Phys. A* **126**(12), 946 (2020a). <https://doi.org/10.1007/s00339-020-04126-9>
- Mudgal, N., Yupapin, P., Ali, J., Singh, G.: BaTiO₃-graphene-affinity layer-based surface plasmon resonance (SPR) biosensor for pseudomonas bacterial detection. *Plasmonics* **15**(5), 1221–1229 (2020b). <https://doi.org/10.1007/s11468-020-01146-2>
- Naresh, V., Lee, N.: A review on biosensors and recent development of nanostructured materials-enabled biosensors. In: *Sensors (Switzerland)*, Vol. **21**, Issue 4, pp. 1–35. MDPI AG. (2021). <https://doi.org/10.3390/s21041109>
- Nesterenko, D. V., Saif-ur-Rehman, Sekkat, Z.: Surface plasmon sensing with different metals in single and double layer configurations. *Appl. Optics*, **51**(27), 6673. (2012). <https://doi.org/10.1364/AO.51.006673>
- Oliveira, L.C., Lima, A.M.N., Thirstrup, C., Neff, H.F.: *Surface Plasmon Resonance Sensors*, vol. 70. Springer International Publishing, Berlin (2019). <https://doi.org/10.1007/978-3-030-17486-6>
- Ong, B.H., Yuan, X., Tjin, S.C., Zhang, J., Ng, H.M.: Optimised film thickness for maximum evanescent field enhancement of a bimetallic film surface plasmon resonance biosensor. *Sens. Actuators, B Chem.* **114**(2), 1028–1034 (2006). <https://doi.org/10.1016/J.SNB.2005.07.064>
- Otto, A.: Excitation of nonradiative surface plasma waves in silver by the method of frustrated total reflection. *Zeitschrift Für Phys. Hadron. Nucl.* **216**(4), 398–410 (1968). <https://doi.org/10.1007/BF01391532>
- Papagiannouli, I., Couris, S., Rioux, D., Meunier, M.: Effect of the composition of Au_xAg_(1-x) nanoalloys on their nonlinear optical response. In: 2013 15th International Conference on Transparent Optical Networks (ICTON), pp. 1–3. (2013). <https://doi.org/10.1109/ICTON.2013.6602747>
- Piliarik, M., Homola, J.: Surface plasmon resonance (SPR) sensors: approaching their limits? *Opt. Express* **17**(19), 16505 (2009). <https://doi.org/10.1364/OE.17.016505>
- Polyanskiy, M. N.: Refractive Index Database. Retrieved January 5, 2024, (n.d.). from <https://refractiveindex.info>
- Querry, M. R.: *Optical constants. US Army Armament, Munitions & Chemical Command, Chemical Research & Development Center.* (1985)
- Raether, H.: *Surface Plasmons on Smooth and Rough Surfaces and on Gratings*, Vol. 111. Springer Berlin Heidelberg. (1988). <https://doi.org/10.1007/BFb0048317>

- Raikwar, S., Srivastava, D.K., Saini, J.P., Prajapati, Y.K.: 2D-antimonene-based surface plasmon resonance sensor for improvement of sensitivity. *Appl. Phys. A* **127**(2), 92 (2021). <https://doi.org/10.1007/s00339-020-04248-0>
- Rioux, D., Vallières, S., Besner, S., Muñoz, P., Mazur, E., Meunier, M.: An analytic model for the dielectric function of Au, Ag, and their alloys. *Adv. Opt. Mater.* **2**(2), 176–182 (2014). <https://doi.org/10.1002/adom.201300457>
- Singh, S., Pandey, S., Yadav, S., Yadav, R.K., Singh, P.K., Lohia, P., Dwivedi, D.K.: Numerical study among Au, Al, and Ag metal-based surface plasmon resonance sensor. *J. Opt.* (2023). <https://doi.org/10.1007/s12596-023-01107-y>
- Singh, S., Sharma, A.K., Lohia, P., Dwivedi, D.K.: Theoretical analysis of sensitivity enhancement of surface plasmon resonance biosensor with zinc oxide and blue phosphorus/MoS₂ heterostructure. *Optik* **244**, 167618 (2021). <https://doi.org/10.1016/j.ijleo.2021.167618>
- Song, B., Li, D., Qi, W., Elstner, M., Fan, C., Fang, H.: Graphene on Au(111): a highly conductive material with excellent adsorption properties for high-resolution bio/nanodetection and identification. *Chem. Phys. Chem.* **11**(3), 585–589 (2010). <https://doi.org/10.1002/cphc.200900743>
- Teng, C., Li, M., Min, R., Deng, S., Chen, M., Xue, M., Yuan, L., Deng, H.: A high-sensitivity SPR sensor based on MMF-tapered HCF-MMF fiber structure for refractive index sensing. *IEEE Sens. J.* **22**(19), 18517–18523 (2022). <https://doi.org/10.1109/JSEN.2022.3201154>
- Tetyana, P., Shumbula, P. M., Njengele-Tetyana, Z.: Biosensors: design, development and applications. In: Ameen, S., Akhtar, M. S., Shin, H.-S. (Eds.), *Nanopores* (p. Ch. 3). IntechOpen. (2021). <https://doi.org/10.5772/intechopen.97576>
- Uniyal, A., Chauhan, B., Pal, A., Srivastava, V.: InP and graphene employed surface plasmon resonance sensor for measurement of sucrose concentration: a numerical approach. *Opt. Eng.* **61**(05), 057103–057103 (2022). <https://doi.org/10.1117/1.OE.61.5.057103>
- Zekriti, M.: Theoretical comparison between graphene-on-silver and gold-on-silver based surface plasmon resonance sensor. *Mater. Today: Proc.* **45**, 7571–7575 (2021). <https://doi.org/10.1016/j.matpr.2021.02.532>
- Zekriti, M., Nesterenko, D.V., Sekkat, Z.: Long-range surface plasmons supported by a bilayer metallic structure for sensing applications. *Appl. Opt.* **54**(8), 2151 (2015). <https://doi.org/10.1364/AO.54.002151>

Publisher's Note Springer Nature remains neutral with regard to jurisdictional claims in published maps and institutional affiliations.

Springer Nature or its licensor (e.g. a society or other partner) holds exclusive rights to this article under a publishing agreement with the author(s) or other rightsholder(s); author self-archiving of the accepted manuscript version of this article is solely governed by the terms of such publishing agreement and applicable law.